Ceramics International 50 (2024) 6403–6411

Contents lists available at ScienceDirect

Ceramics International

journal homepage: www.elsevier.com/locate/ceramint

Structure characteristics and microwave/terahertz dielectric response of low-permittivity $(La_{0.2}Nd_{0.2}Sm_{0.2}Eu_{0.2}Gd_{0.2})_2Zr_3(MoO_4)_9$ high-entropy ceramics

Huanrong Tian [a,b,c], Xiaohan Zhang [b], Wei Du [b], Zhanbai Feng [d], Laiguo Wang [a,**], Haitao Wu [b,*], Wangsuo Xia [e,***]

[a] Anhui Key Laboratory of Photoelectric-Magnetic Functional Materials, Anhui Key Laboratory of Functional Coordination Compounds, Anqing Normal University, Anqing, 246011, China
[b] Yantai University, Yantai, 264005, Shandong, China
[c] Key Laboratory for Liquid-Solid Structural Evolution and Processing of Materials (Ministry of Education), Shandong University, Jinan 250061, China
[d] School of Materials Science and Engineering, University of Jinan, Jinan, 250022, China
[e] School of Materials Science and Physics, China University of Mining and Technology, Xuzhou 221116, China

ARTICLE INFO

Keywords:
Microwave dielectric properties
$(La_{0.2}Nd_{0.2}Sm_{0.2}Eu_{0.2}Gd_{0.2})_2Zr_3(MoO_4)_9$ high-entropy ceramics
Complex chemical bond theory
Terahertz time-domain spectroscopy

ABSTRACT

Microwave dielectric ceramics play a vital role in wireless communication systems. However, it is a great challenge to obtain ideal performances of single-phase ceramics. In this work, $(La_{0.2}Nd_{0.2}Sm_{0.2}Eu_{0.2}Gd_{0.2})_2Zr_3(MoO_4)_9$ (abbreviated as L5ZMO) high-entropy ceramics were successfully prepared by the solid-state reaction method, the pure trigonal L5ZMO structure can be synthesized in the mixture calcined at 700 °C. Rietveld refinement based on XRD data reveals that lattice parameters of L5ZMO ceramics are affected by the radius of the five rare earth elements, which indicates that the rare earth elements have been solubilized and randomly distributed in the Ln-site. The relative density illustrates a strong dependence on sintering temperature, which gradually increases with increasing sintering temperature. Based on the analysis of bond characteristics, the Mo–O bond exhibits a vital effect on the dielectric properties of L5ZMO ceramics. Besides, the infrared reflection spectrum and terahertz time-domain spectroscopy analysis show that ionic polarization is the dominant polarization in the microwave/terahertz bands. Meanwhile, the tan δ can be further reduced by optimizing process parameters. Notably, the L5ZMO high-entropy ceramics sintered at 750 °C exhibit outstanding dielectric properties of $\varepsilon_r = 10.46$, $Q{\cdot}f = 59{,}713$ GHz, and $\tau_f = -21.94$ ppm/°C, indicating that the high-entropy design optimizes τ_f (−38.8 ppm/°C) of the simple $La_2Zr_3(MoO_4)_9$ ceramics. The attempt provides theoretical guidance for the application of high-entropy design concepts in microwave/terahertz bands.

1. Introduction

The new generation of wireless communication systems (5G or even 6G) needs high performance microwave devices to provide more reliable, faster signal transmission, and larger storage capacity. Massive Multiple-Input Multiple-Output technology greatly improve the signal processing efficiency of communication equipment [1]. Therefore, microwave dielectric ceramics, as the key material of filters, capacitors, duplexers, and antennas, have been put forward higher performance requirements [2–5], including low sintering temperature provides the possibility of modularity for the device [6–8]; low dielectric constant (ε_r) to ensure a low delay of the signal [9–11], high quality factor ($Q{\cdot}f$) to guarantee the reliability of the signal [12], a near-zero temperature coefficient of the resonant frequency (τ_f) to minimze the fluctuation of the resonance frequency with change in temperature of the environment [13]. However, these microwave dielectric parameters are mutually restricted, and it is difficult to obtain ideal value simultaneously. Thus, few ceramics systems can meet these requirements. Microwave dielectric ceramics with low ε_r are usually accompanied by a larger negative τ_f, and superimposing the second phase with a positive τ_f is a common

* Corresponding author.
** Corresponding author.
*** Corresponding author.
E-mail addresses: wanglg@aqnu.edu.cn (L. Wang), wuhaitao@ytu.edu.cn (H. Wu), xiaws@cumt.edu.cn (W. Xia).

https://doi.org/10.1016/j.ceramint.2023.11.378
Received 27 June 2023; Received in revised form 28 November 2023; Accepted 29 November 2023
Available online 3 December 2023

solution, but the quality factor will inevitably deteriorate [14,15]. Hence, it urges us to explore new material design concepts to break the constraints of $Q{\cdot}f$ and τ_f.

Recently, high-entropy ceramics have been proposed as a new material design strategy, which are solid solution ceramics with multiple elements sharing the equivalent lattice sites. The concept is derived from high-entropy alloys, the appearance of high-entropy ceramics opens up a new field and provides a direction for the design of high performance ceramics [16–23]. Ye [17] and Zhao [18] reported that the mechanical properties of $(Zr_{0.25}Nb_{0.25}Ti_{0.25}V_{0.25})C$ and $(La_{0.2}Sm_{0.2}Eu_{0.2}Gd_{0.2}Tm_{0.2})_2Zr_2O_7$ ceramics were significantly improved. Moreover, $(La_{0.2}Nd_{0.2}Sm_{0.2}Gd_{0.2}Yb_{0.2})_2Zr_2O_7$ ceramics exhibited excellent high-temperature thermal stability, which presented great application potential in thermal barrier coatings [19]. In the attempt of Li $(Gd_{0.2}Ho_{0.2}Er_{0.2}Yb_{0.2}Lu_{0.2})GeO_4$ system, the near-zero τ_f (−7.4 ppm/°C) was received [20]. Currently, Lin et al. reported the mechanical and dielectric properties of $SrLaAlO_4$ ceramics can be effectively improved by high-entropy design [23]. Therefore, the design of high-entropy ceramics is of great significance for the improvement of dielectric and mechanical properties.

In the last few years, $Ln_2(MoO_4)_3$–$Zr(MoO_4)_2$ molybdate systems have been systematically reported [24–29]. Thereinto, the $La_2Zr_3(MoO_4)_9$ ceramics showed low ε_r (10.80), excellent $Q{\cdot}f$ (50,628 GHz), and low sintering temperature (775 °C), which presented good application potential in high-frequency wireless communication. However, the large negative τ_f (−38.8 ppm/°C) dramatically limited their practical applications. Inspired by high-entropy ceramics, the equimolar-ratio Nd, Sm, Eu, and Gd elements were introduced into Ln-site forming high-entropy ceramics to modify temperature stability, with the nominal composition of $(La_{0.2}Nd_{0.2}Sm_{0.2}Eu_{0.2}Gd_{0.2})_2Zr_3(MoO_4)_9$. In this work, the L5ZMO ceramics were fabricated through a solid-state reaction route, the phase structure, microstructure and dielectric properties have been intensively explored. Besides, the terahertz time-domain spectroscopy (THz-TDS) was carried out to observe the performance of high-entropy ceramics at terahertz frequencies. Those experimental results provide practical and theoretical guidance for high-entropy ceramics under microwave/terahertz application.

2. Experimental methods

$(La_{0.2}Nd_{0.2}Sm_{0.2}Eu_{0.2}Gd_{0.2})_2Zr_3(MoO_4)_9$ powder was fabricated by the solid-state reaction method. Zirconia ball was used as grinding media, high-purity raw materials La_2O_3 (99.99%), Sm_2O_3 (99.9%), Nd_2O_3 (99.99%), Gd_2O_3 (99.9%), Eu_2O_3 (99.99%), ZrO_2 (99.9%), and MoO_3 (99.5%) were weighed at the ratio of 1:1:1:1:1:15:45 and ball-milled for 10 h to obtain uniform mixture. After drying, the mixed powder was calcined at 650 °C and 700 °C for 2 h. Then, the calcined powder was re-milled, dried, and sieved again before granulation. Subsequently, the powder with 11% paraffin was condensed into cylindrical pellets (Φ = 10 mm, H = 5–6 mm) at the uniaxial pressure of 600 MPa. The green bodies were held at 500 °C for 4 h to remove the binder and then sintered at 700–800 °C for 6 h in the air.

The structure of calcined powder and sintered ceramics were confirmed using X-ray diffractometer (XRD, SmartLab). Apparent and relative density were measured based on the Archimedes method, and the cell volume was refined by the FULLPROF module. The scanning electron microscope (SEM, FEI QUANTA FEG 250) equipped with an energy-dispersive spectroscope (EDS, INCA Energy X-MAX-50) was used to detect the morphology and element distribution. The microwave dielectric properties were measured by a vector network analyzer (Agilent N5234A) and a temperature chamber (BPH-120A). The ε_r value was measured using the Hakki-Coleman method modified by Courtney [30,31], and the $Q{\cdot}f$ value was evaluated by the $TE_{01\delta}$ cavity method [32,33]. The τ_f value of the sample was measured in the temperature range from 25 °C to 85 °C. The terahertz time-domain spectroscopy was performed using a terahertz time-domain spectrometer system (Z3). Bruker IFS 66v FTIR spectrometer was used to record the infrared reflection spectrum.

3. Results and discussion

Fig. 1(a) presents the XRD patterns of the mixture powder calcined at 650 °C and 700 °C for 2 h. The diffraction peaks of MoO_3 and $Zr(MoO_4)_2$ can be detected at 650 °C, indicating that the synthesis of the L5ZMO phase is based on $Zr(MoO_4)_2$ as an intermediate product, rather than a simple one-step chemical reaction. The specific reaction equations are shown in Eq. (1) and Eq. (2).

$$ZrO_2 + 2MoO_3 \rightarrow Zr(MoO_4)_2 \quad (1)$$

$$3Zr(MoO_4)_2 + Ln_2O_3 + 3MoO_3 \rightarrow Ln_2Zr_3(MoO_4)_9 \quad (2)$$

Correspondingly, the rare earth oxide should also be found at 650 °C, yet no obvious rare earth oxides diffraction peak is indexed, which may be due to the insufficient accuracy of XRD, so a small amount of rare earth oxides diffraction peak (Sm_2O_3, Nd_2O_3, and La_2O_3) overlaps in the L5ZMO structure. When the calcining temperature rises to 700 °C, the chemical reaction among oxides is complete, and the pure L5ZMO phase can be obtained. In addition, Fig. 1(a) also displays the XRD patterns of L5ZMO ceramics sintered at 700–800 °C. All diffraction peaks are identified as the trigonal $Sm_2Zr_3(MoO_4)_9$ structure with R-3c symmetry (PDF#52–0639), indicating that the rare earth oxides have been absolutely incorporated into the L5ZMO structure to form solid solution ceramics.

To get a clear understanding of the structure characteristics, Rietveld refinements were conducted by the FULLPROF module based on the XRD data, which were derived from L5ZMO samples sintered at 750 °C. The homotypic $Nd_2Zr_3(MoO_4)_9$ structure is used as the starting model, and the refined results of the specimen are depicted in Fig. 1(b). The calculated values match well with the observed one, and the reliability factors are $\chi^2 = 2.08$, $R_p = 4.06\%$, $R_{wp} = 5.31\%$, $R_{exp} = 3.68\%$, the smooth blue line (difference between measured and calculated values) and the low R-factors (<15%) suggested that the refined result was credible. The lattice parameters $a = b = 9.8013$ Å, $c = 58.3847$ Å are collected in Table 1. Furthermore, the lattice parameters of $Ln_2Zr_3(MoO_4)_9$ (Ln = La, Nd, Sm, Eu, Gd) systems are also listed, and the data are obtained from the ICSD database and the PDF card. The high-entropy ceramics exhibit a medium abc and cell volume (V), which is due to the co-occupation of La^{3+} ($r = 1.22$ Å), Nd^{3+} ($r = 1.16$ Å), Sm^{3+} ($r = 1.13$ Å), Eu^{3+} ($r = 1.12$ Å), Gd^{3+} ($r = 1.11$ Å) elements at the Ln-site [34]. Fig. 1(c) plots a schematic diagram of the L5ZMO structure, which consists of $[LnO_9]$ tetrakaidekahedron, $[ZrO_6]$ octahedron, and $[MoO_4]$ tetrahedron, five rare earth elements occupy the Ln-site uniformly and randomly. In the L5ZMO structure, polyhedrons of the same type are isolated from each other, the $[MoO_4]$ tetrahedron serves as a bridge, and each $[MoO_4]$ tetrahedron is linked with two $[LnO_9]$ tetrakaidekahedron and two $[ZrO_6]$ octahedron by corner sharing.

Fig. 2 exhibits the density of the L5ZMO ceramics sintered at different temperatures. The apparent and relative density gradually increase as the sintering temperature increases, reaching the maximum relative density of 95.1% at 800 °C, which may be ascribed to the gradual elimination of pores. In order to confirm the speculation, the cross-sectional morphology of L5ZMO ceramics is examined and illustrated in Fig. 3. Distinct pores can be observed in Fig. 3(a) sintered at 700 °C. When the sintering temperature rises to 725 °C, the visible pores gradually disappear, but there are still fine pores. With the further increases of sintering temperature, the L5ZMO ceramics present a relatively dense microstructure. Thus, the reduced pores are one of the reasons for improving the density of ceramics specimens. In addition, the grain sizes of L5ZMO ceramics are measured by Nano Measurer and embedded in the corresponding SEM images, the mean grain sizes are located in 1.58–1.78 μm, which presents slight dependence on the whole temperature range. In order to more intuitively confirm whether the

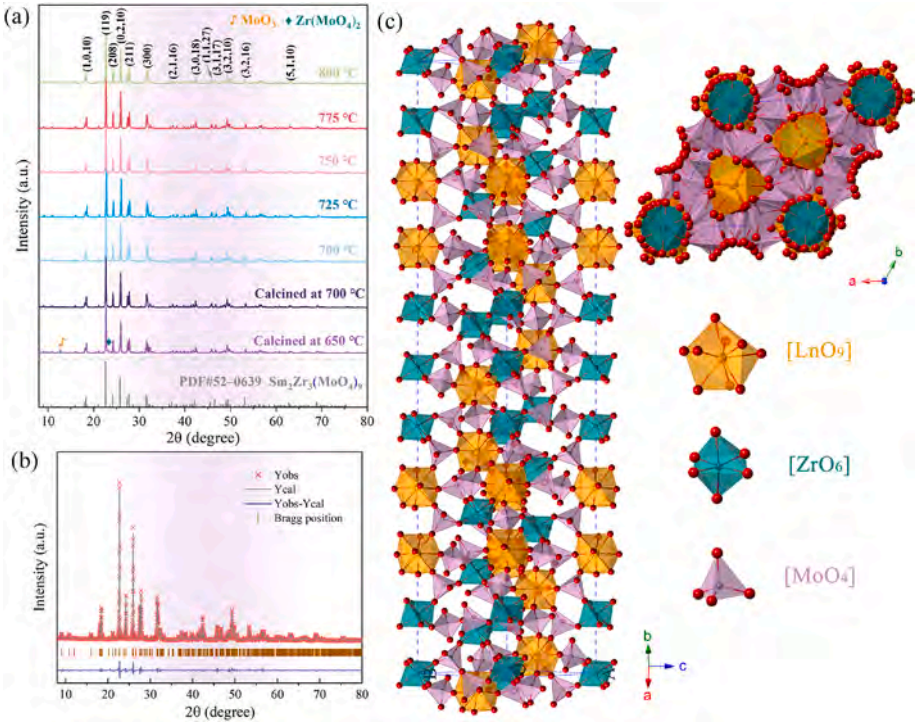

Fig. 1. (a) XRD patterns of the mixture powder calcined at 650 °C, 700 °C and L5ZMO high-entropy ceramics sintered at 700–800 °C, (b) the refinement patterns of L5ZMO ceramics sintered at 750 °C, and (c) schematic diagram of L5ZMO structure.

Table 1
The lattice parameters of $Ln_2Zr_3(MoO_4)_9$ (Ln = La, Nd, Sm, Eu, Gd) systems and L5ZMO high-entropy ceramics.

Compound	$a = b$ (Å)	c (Å)	V (Å^3)	Source
$La_2Zr_3(MoO_4)_9$	9.8463	59.0970	4961.83	PDF#52-0688
$Nd_2Zr_3(MoO_4)_9$	9.8040	58.4670	4866.86	ICSD-92600
$Sm_2Zr_3(MoO_4)_9$	9.7949	58.2280	4837.96	PDF#52-0639
$Eu_2Zr_3(MoO_4)_9$	9.7852	58.0710	4815.37	PDF#53-0172
$Gd_2Zr_3(MoO_4)_9$	9.7760	57.9310	4794.73	PDF#54-0052
L5ZMO	9.8013	58.3847	4857.42	This work

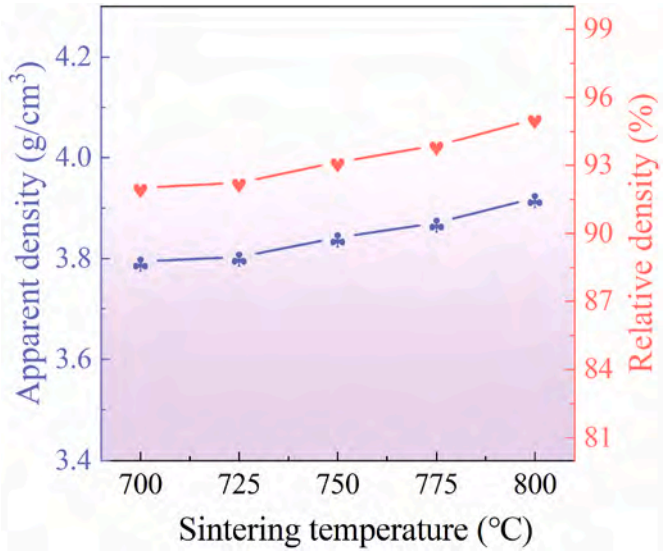

Fig. 2. The apparent and relative density of the L5ZMO ceramics with sintering temperature.

elements of L5ZMO high-entropy ceramics are in accordance with the original set proportion, EDS mapping was performed and plotted in Fig. 3(f), each element exhibits a random, uniform arrangement in the high-entropy ceramics. The rare earth elements have equimolar ratio, the ratio of La + Nd + Sm + Eu + Gd:Zr:Mo:O = 3.80:5.69:16.71:73.8 are consistent with $(La_{0.2}Nd_{0.2}Sm_{0.2}Eu_{0.2}Gd_{0.2})_2Zr_3Mo_9O_{36}$. Consistent with XRD results, it is further proved that the rare earth elements have successfully entered the Ln-site lattice to form a solid solution ceramic.

The microwave dielectric properties of L5ZMO high-entropy ceramics with different sintering temperatures are presented in Fig. 4. With the increase of sintering temperature, the ε_r values increase gradually from 10.21 to 10.68, the trend is in line with that of the relative density, demonstrating that the ε_r value of L5ZMO ceramics is affected by the density. To further investigate the influence factor of ε_r, the Bosman-Having's way was applied to correct the ε_r value [35].

$$\varepsilon\text{corr.} = \varepsilon\text{mea.}(1 + 1.5P) \tag{3}$$

where P is the fractional porosity. The $\varepsilon_{corr.}$ values at different sintering temperatures are presented in Fig. 4(a), the $\varepsilon_{corr.}$ value are almost identical throughout the sintering temperatures range, the maximum ε_{corr} can be obtained in the L5ZMO ceramics sintered at 750 °C. Furthermore, the Clausius-Mossotti equation shows that the ε_r value is related to ionic polarizability (α_D).

$$\mathrm{b}\frac{\alpha_D}{V} = 1 - \frac{3}{2 + \varepsilon_r} \tag{4}$$

where b and V are constant value ($4\pi/3$) and molar volume, respectively. Shannon [36] proposed that molecular polarizability (α_D) can be calculated by the sum of the constituent ions, for $(La_{0.2}Nd_{0.2}Sm_{0.2}Eu_{0.2}Gd_{0.2})_2Zr_3(MoO_4)_9$:

$$\alpha_{L5ZMO} = 2 \times 0.2 \times (\alpha_{La^{3+}} + \alpha_{Nd^{3+}} + \alpha_{Sm^{3+}} + \alpha_{Eu^{3+}} + \alpha_{Gd^{3+}}) + 3\alpha_{Zr^{4+}} + 9\alpha_{Mo^{6+}} + 36\alpha_{O^{2-}} \tag{5}$$

where the ionic polarizability of La^{3+}, Nd^{3+}, Sm^{3+}, Eu^{3+}, Gd^{3+}, Zr^{4+}, Mo^{6+}, and O^{2-} are 6.07 Å^3, 5.01 Å^3, 4.74 Å^3, 4.53 Å^3, 4.37 Å^3, 3.25 Å^3,

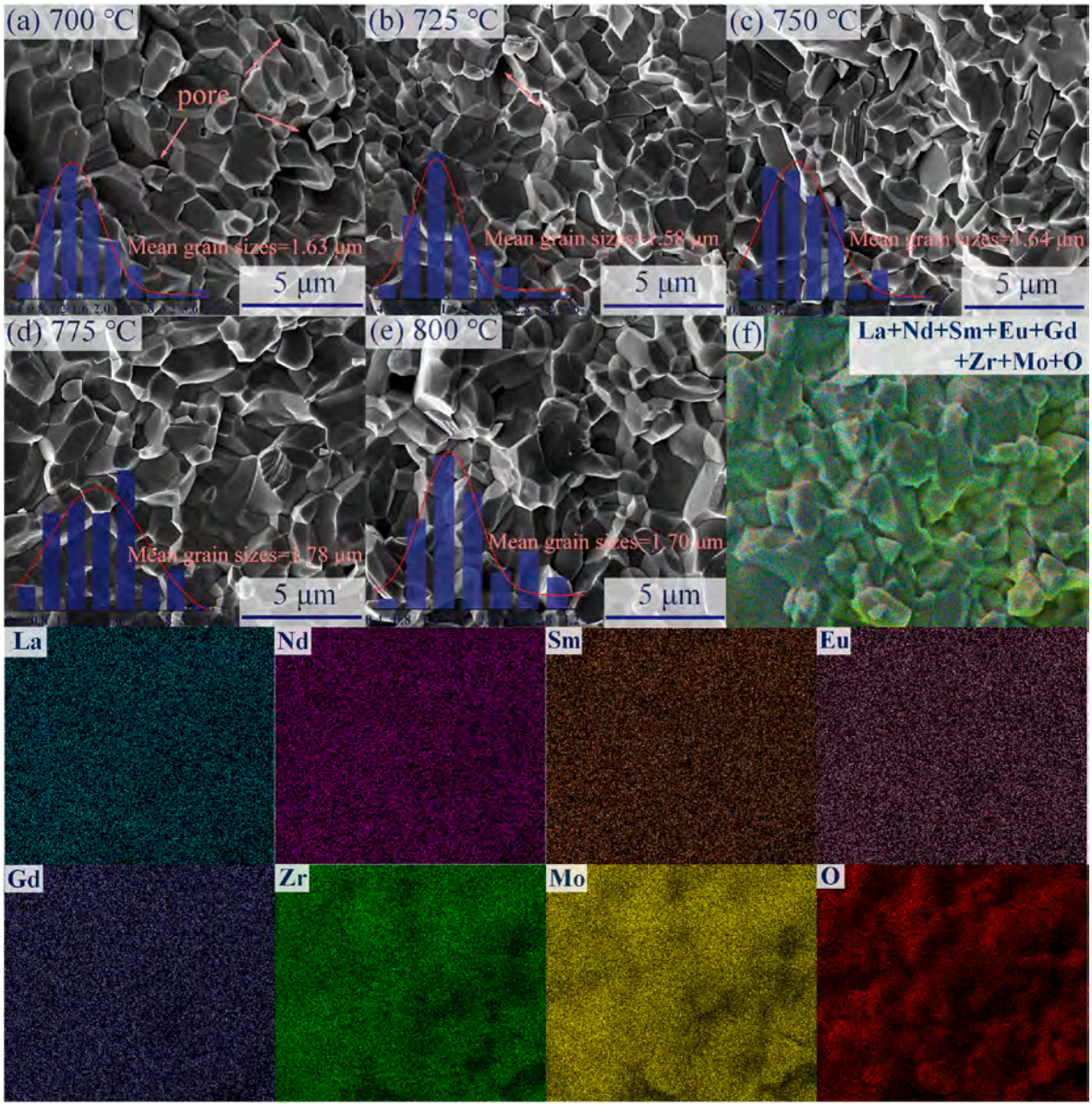

Fig. 3. The cross-sectional morphology of L5ZMO high-entropy ceramics sintered at different temperatures (a) 700 °C, (b) 725 °C, (c) 750 °C, (d) 775 °C, (e) 800 °C, (f) EDS mapping of L5ZMO high-entropy ceramics sintered at 750 °C, including holistic EDS mapping and EDS mappings of La, Nd, Sm, Eu, Gd, Zr, Mo and O elements. The inset illustration is a grain size distribution map.

3.28 Å^3, and 2.01 Å^3, respectively [37,38]. Moreover, the α_D/V and corrected ε_r value of $Ln_2Zr_3(MoO_4)_9$ systems are listed in Table 2 [24–27]. The L5ZMO high-entropy ceramics present medium α_D/V and $\varepsilon_{corr.}$ value, indicating that the ε_r value is greatly affected by α_D/V.

As shown in Fig. 4(b), the $Q{\cdot}f$ value of L5ZMO ceramics gradually increases to the maximum value of 59,713 GHz at 750 °C, which is higher than that of $La_2Zr_3(MoO_4)_9$ ceramics (50,628 GHz) [24]. When the sintering temperature rises to 800 °C, the $Q{\cdot}f$ value of L5ZMO ceramics drops to 48,319 GHz. Generally, the $Q{\cdot}f$ value is sensitive to the extrinsic factors such as secondary phases, porosity, and grain boundary. Combined with XRD results, the impurities can be excluded. The rising trend of $Q{\cdot}f$ value is same as that of the relative density, indicating that the density has a primary influence on the $Q{\cdot}f$ value compared with other extrinsic factors. The subsequent decrease in $Q{\cdot}f$ value should be ascribed to excessive temperature. In addition, τ_f is another crucial parameter for microwave dielectric ceramics. According to Fig. 4(b), the absolute value of τ_f for L5ZMO high-entropy ceramics decreases gradually from 30.45 to 21.94 and then increases to 23.34 with an increase of sintering temperature. In general, the τ_f values are kept at −25 ppm/°C, which shows that L5ZMO high-entropy ceramics possess outstanding temperature stability compared with $La_2Zr_3(MoO_4)_9$ ceramics [24], confirming the feasibility of the high-entropy design. Notably, excellent microwave dielectric properties ($\varepsilon_r = 10.46$, $Q{\cdot}f = 59{,}713$ GHz, and $\tau_f = -21.94$ ppm/°C) are obtained in the L5ZMO high-entropy ceramics sintered at 750 °C.

The complex chemical bond theory is a useful tool to calculate the properties of chemical bonds. This theory makes it possible to quantify the contribution of fundamental variables (bond ionicity, lattice energy, and bond energy) to the variation of dielectric properties [39–42]. Therefore, the complex chemical bond theory is considered to be a feasible method to evaluate the correlations between bond characteristics and performances, and the detailed formulas can be found in our previous reports [43–45]. Based on the crystal structure of L5ZMO ceramics and Zhang's decomposition method [39], the complex polycrystal of $(La_{0.2}Nd_{0.2}Sm_{0.2}Eu_{0.2}Gd_{0.2})_2Zr_3(MoO_4)_9$ is converted to a sum of binary bonding formulas:

$$(La_{0.2}Nd_{0.2}Sm_{0.2}Eu_{0.2}Gd_{0.2})_2Zr_3(MoO_4)_9 = La/Nd/Sm/Eu/Gd_2Zr1Zr2_2Mo1_6Mo2_3O1_6O2_6O3_6O4_6O5_6O6_6 = La/Nd/Sm/Eu/Gd_{2/3}O1_3+La/Nd/Sm/Eu/Gd_{2/3}O2_3+La/Nd/Sm/Eu/Gd_{2/3}O6_3 +Zr1O4_3+Zr2O3_3+Zr2O5_3+Mo1_{3/2}O1_3+Mo1_{3/2}O2_3+Mo1_{3/2}O3_3+Mo1_{3/2}O4_3 +Mo2_{3/2}O5_3+Mo2_{3/2}O6_3 \quad (6)$$

The bond ionicity (f_i), lattice energy (U), coefficient of thermal expansion (α), and bond energy (E) have been calculated and illustrated in Fig. 5, and the detailed values are collected in Table 3. Furthermore, the inherent relationship between ε_r and f_i can be evaluated by Eq. (7) [46].

$$\varepsilon_r = \frac{n^2-1}{1-f_i}+1 \quad (7)$$

where n represents the refractive index. As shown in Fig. 5(a), the f_i of the Mo–O bond has the largest proportion of bond ionicity, which indicates that the Mo–O bond has a great impact on ε_r. The lattice energy is the binding capacity between anions and cations, which is related to crystal stability. It can be seen that the U of the Mo–O bond has a higher order of magnitude in Fig. 5(b), indicating that the Mo–O bond offers great lattice stability and is more conducive to the improvement of $Q{\cdot}f$ value. As shown in Figs. 5(c) and Fig. 4(b), the α_l of the Mo–O bond and τ_f present negative values. According to the inverse correlation between α_l and τ_f shown in Eq. (8), the α_l of the Mo–O bond exhibits a positive impact on τ_f values.

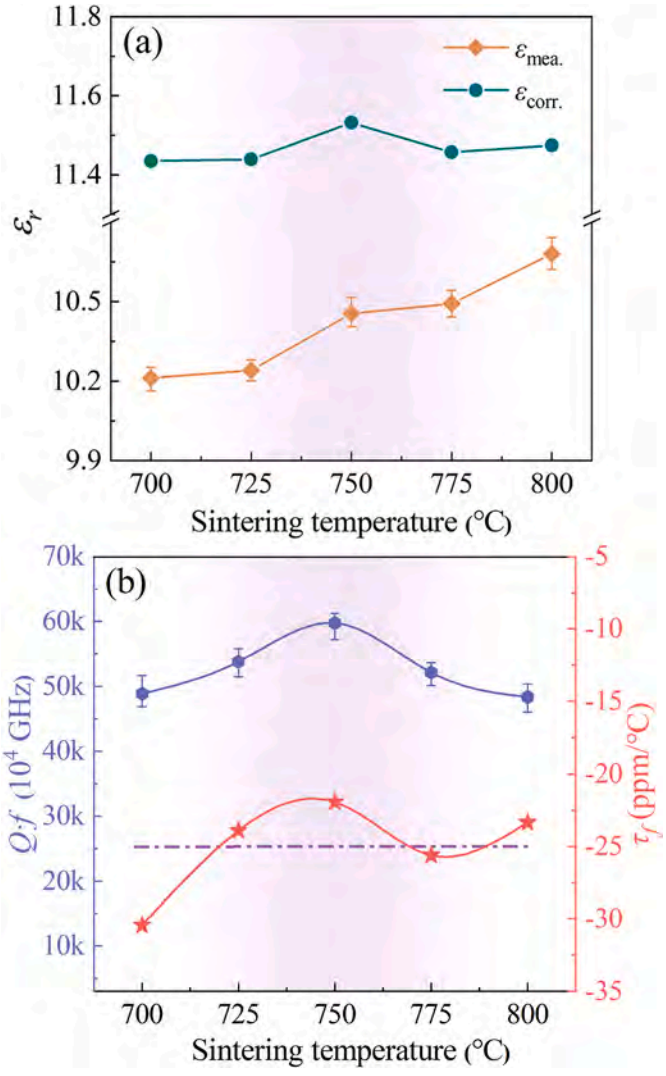

Fig. 4. (a) Measured and corrected ε_r values, (b) $Q{\cdot}f$ andτ_f of L5ZMO high-entropy ceramics as a function of sintering temperature.

$$\tau_f = -\left(\alpha_l + \frac{1}{2}\tau_\varepsilon\right) \quad (8)$$

In addition, the E of the Mo–O bond accounts for a major part of the total E, indicating that the Mo–O bond has a relatively strong impact on the thermal stability of L5ZMO ceramics. In conclusion, the Mo–O bond is essential for the microwave dielectric properties of L5ZMO high-entropy ceramics.

The dielectric properties at terahertz frequency regions were achieved by THz-TDS. Fig. 6 displays the optical and dielectric properties of L5ZMO high-entropy ceramics sintered at 750 °C. With the frequency increases from 0.5 THz to 1.5 THz, the refractive index (n) and dielectric constant (ε') of L5ZMO ceramics increase slowly, while the absorption coefficient (α) and dielectric loss (tan δ) increase continuously, which is aligned with the tendency of other microwave dielectric ceramics in the THz region reported previously [47–49]. Typically, the ε' of L5ZMO ceramics at 13.0 GHz and 1 THz are 10.46 and 10.16, respectively. The slight deviation may be caused by insufficient surface polishing of the test sample [50]. Meantime, the close ε' suggests that the polarization mechanism of L5ZMO ceramics at terahertz and microwave frequencies remains unchanged, which originates from ionic polarization and electron polarization [51]. Besides, based on the dispersion theory, the tan δ is defined as the ratio of the real and imaginary parts of the complex dielectric constant, as shown in Eq. (9):

$$\tan\delta = \frac{\varepsilon''}{\varepsilon'} \approx \frac{\gamma\omega}{\omega_T{}^2} \quad (9)$$

where γ is damping factor, and ω_T represents transverse optic mode frequency. Hence, the slope of the linear fit of tan δ as a function of frequency can represent the γ of the lattice vibration, and the slope of the linear fit of tan δ for L5ZMO ceramics in Fig. 6(d) is 0.024. Furthermore, the L5ZMO ceramics sintered at 750 °C exhibit outstanding optical and dielectric properties at 0.5 THz: n = 3.19, α = 10.37 cm^{-1}, ε' = 10.16, and tan δ = 0.016, which is expected to be an ideal material for terahertz band dielectric substrates for its low ε_r and tan δ values.

To further study the intrinsic dielectric response of L5ZMO high-entropy ceramics, the infrared reflection spectrum analysis of ceramics sample sintered at 750 °C was conducted. As displayed in Fig. 7(a), the

Table 2
The polarizability per unit volume (α_D/V), measured and corrected ε_r values of $Ln_2Zr_3(MoO_4)_9$ (Ln = La, Nd, Sm, Eu, Gd) systems and L5ZMO high-entropy ceramics.

Compound	ε_r	$\varepsilon_{corr.}$	α_D/V	References
$La_2Zr_3(MoO_4)_9$	10.80	11.01	0.02494	[16]
$Nd_2Zr_3(MoO_4)_9$	10.80	11.21	0.02500	[17]
$Sm_2Zr_3(MoO_4)_9$	11.00	11.50	0.02503	[17]
$Eu_2Zr_3(MoO_4)_9$	10.75	11.54	0.02506	[18]
$Gd_2Zr_3(MoO_4)_9$	11.17	12.01	0.02510	[19]
L5ZMO	10.46	11.53	0.02502	This work

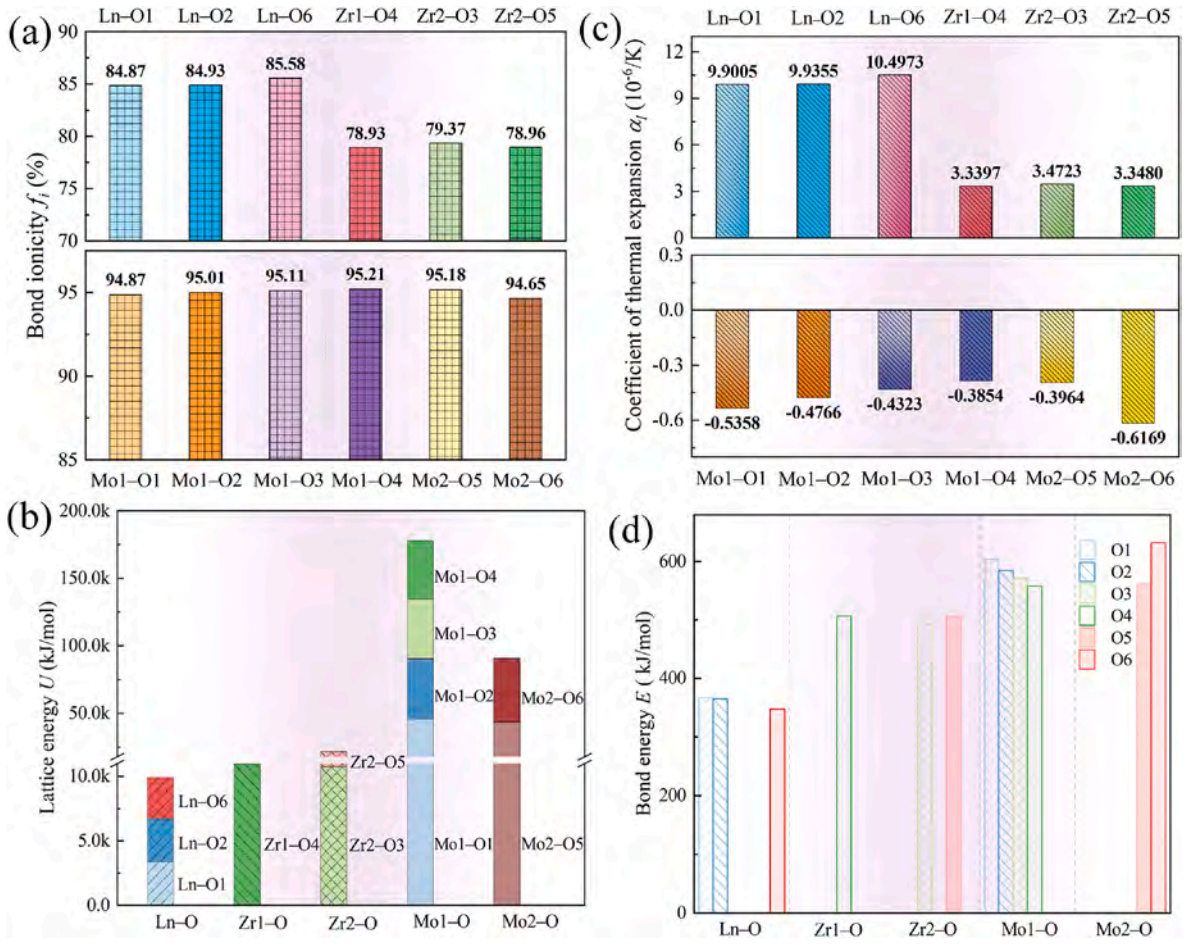

Fig. 5. (a) Bond ionicity (f_i), (b) lattice energy (U), (c) coefficient of thermal expansion (α), and (d) bond energy (E) of L5ZMO high-entropy ceramics.

Table 3
Bond ionicity (f_i), lattice energy (U), coefficient of thermal expansion (α), and bond energy (E) values of L5ZMO high-entropy ceramics.

Bond type	f_i (%)	U (kJ/mol)	α_l (10^{-6}/K)	E (kJ/mol)
Ln–O1	84.87	1122	9.9005	366.75
Ln–O1	84.87	1122	9.9005	366.68
Ln–O1	84.87	1122	9.9005	366.60
Ln–O2	84.93	1119	9.9355	365.11
Ln–O2	84.93	1119	9.9355	365.06
Ln–O2	84.93	1119	9.9355	365.00
Ln–O6	85.58	1073	10.4973	347.54
Ln–O6	85.58	1073	10.4973	347.49
Ln–O6	85.59	1073	10.4973	347.44
Zr1–O4	78.93	10,966	3.3397	506.47
Zr2–O3	79.37	3583	3.4711	493.57
Zr2–O3	79.37	3582	3.4729	493.43
Zr2–O3	79.37	3582	3.4729	493.38
Zr2–O5	78.96	3651	3.3474	505.70
Zr2–O5	78.96	3651	3.3474	505.63
Zr2–O5	78.97	3650	3.3492	505.48
Mo1–O1	94.87	45,746	−0.5358	603.68
Mo1–O2	95.01	44,739	−0.4766	584.71
Mo1–O3	95.11	44,015	−0.4323	571.38
Mo1–O4	95.21	43,273	−0.3854	557.96
Mo2–O5	95.18	43,445	−0.3964	561.05
Mo2–O6	94.65	47,200	−0.6169	632.01

infrared reflection spectrum fitted by 20 Lorentz modes match well with the observed one [52], and the phonon parameters are tabulated in Table 4.

$$\varepsilon^*(\omega) = \varepsilon_\infty + \sum_{j=1}^{n} \frac{{\omega_{pj}}^2}{{\omega_{oj}}^2 - \omega^2 - j\gamma_j\omega} \tag{10}$$

$$R(\omega) = \left| \frac{1 - \sqrt{\varepsilon^*(\omega)}}{1 + \sqrt{\varepsilon^*(\omega)}} \right|^2 \tag{11}$$

where the ω_{oj} and ω_{pj} denote transverse and plasma frequency, respectively. Since the microwave frequency ω is much lower than ω_{oj}, Eq. (10) can be simplified as [53]:

$$\varepsilon' = \varepsilon_\infty + \sum_{j=1}^{n} \frac{\omega_{pj}^2}{\omega_{oj}^2} = \varepsilon_\infty + \sum_{j=1}^{n} \Delta\varepsilon_j \tag{12}$$

As reported in $La_2Zr_3(MoO_4)_9$ and $Eu_2Zr_3(MoO_4)_9$ systems [26,54], the number of fitted modes is slightly less than the number predicted by group theory, which may be due to measurement accuracy, overlap, and degeneracy [55].

As shown in Fig. 7(b), it can be seen that the calculated value of ε_r (8.01) is less than the measured one (10.46), which may include the

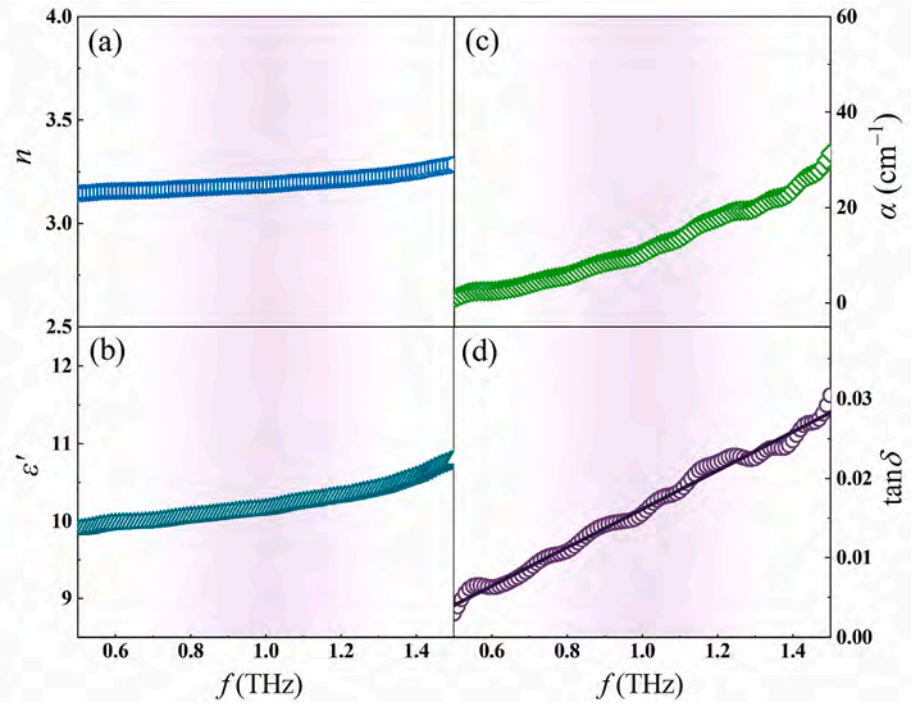

Fig. 6. (a) Refractive index (n), (b) dielectric constant (ε'), (c) absorption coefficient (α), and (d) dielectric loss (tan δ) of L5ZMO high-entropy ceramics.

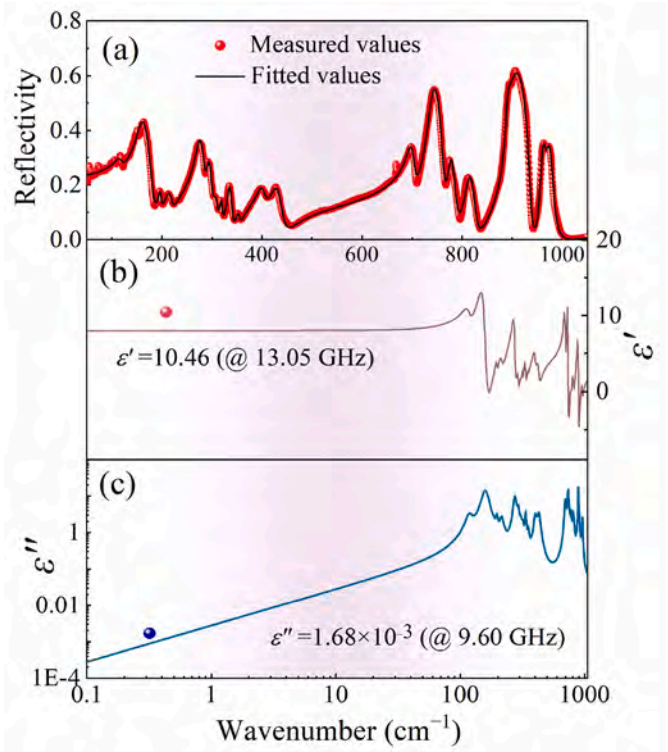

Fig. 7. (a) Measured and fitted infrared reflection spectrum, (b) the real parts of the calculated and measured complex permittivity, and (c) the imaginary parts of the calculated and measured complex permittivity for L5ZMO high-entropy ceramics.

polarization contribution of defective phonon scattering [51,56,57]. On the other hand, it is well-known that the extrapolated value of dielectric properties to microwave frequencies from infrared reflection spectrum is sensitive to roughness of the test sample. Hence, the deviation may be caused by the diffuse reflection of pores in the test sample. Besides, optical frequency polarization of 38.70% and ionic polarization of 61.30% are obtained in the calculated ε_r, indicating that the ionic polarization provides the main contribution to the ε_r of the L5ZMO high-entropy ceramics. Meanwhile, the tan δ is extrapolated by Eq. (13) [58]:

$$\tan\delta = \frac{\varepsilon''}{\varepsilon'} = \frac{\sum_{j=1}^{n} \Delta\varepsilon_j (\gamma_j \omega) \Big/ \omega_{oj}^2}{\varepsilon_\infty + \sum_{j=1}^{n} \Delta\varepsilon_j} \tag{13}$$

The results are collected in Table 4, where the vibration modes below 400 cm^{-1} contribute 72.30% of the dielectric polarization and 97.23%

Table 4
Phonon parameters and dielectric loss for L5ZMO high-entropy ceramics.

j	ω_{oj} (cm^{-1})	ω_{pj} (cm^{-1})	γ_j (cm^{-1})	$\Delta\varepsilon_j$	tan $\delta_j \times 10^4$
1	118.54	69.38	19.08	0.3430	0.18565
2	159.12	230.22	24.18	2.0900	0.79558
3	196.63	46.04	6.77	0.0548	0.00382
4	215.44	82.77	16.64	0.1480	0.02116
5	274.71	207.94	16.92	0.5730	0.05123
6	292.81	112.87	12.14	0.1490	0.00841
7	307.14	69.76	11.56	0.0516	0.00252
8	318.34	52.65	5.69	0.0273	0.00061
9	335.29	101.83	9.59	0.0922	0.00314
10	353.18	51.59	8.53	0.0213	0.00058
11	400.45	146.79	20.94	0.1340	0.00698
12	427.72	192.85	26.93	0.2030	0.01191
13	698.18	299.46	17.10	0.1840	0.00257
14	736.43	473.88	17.69	0.4140	0.00538
15	774.62	192.76	16.59	0.0619	0.00068
16	811.46	236.97	21.17	0.0853	0.00109
17	888.80	333.81	8.98	0.1410	0.00064
18	894.44	284.99	22.04	0.1020	0.00112
19	956.18	169.46	11.07	0.0314	0.00015
20	968.90	56.59	11.15	0.0034	0.00002
ε_∞				3.0996	0
$\sum$				8.0098	1.10325

of the dielectric loss, suggesting that the phonon vibration modes in the low wave-number band are particularly important for the dielectric properties. Besides, the calculated $Q{\cdot}f$ (86,835 GHz) value is higher than the measured one (59,713 GHz), indicating that the $Q{\cdot}f$ value is affected by extrinsic factors [51], and a better $Q{\cdot}f$ value can be obtained via adjusting process parameters.

4. Conclusions

A novel L5ZMO high-entropy ceramics were successfully prepared by the solid-state method. Further, crystal phase, microstructure, and microwave dielectric properties of L5ZMO high-entropy ceramics were systematically studied. The XRD results illustrate that trigonal structure is synthesized at 700 °C. The refinement results further reveal that lattice parameters are affected by the radius of the five rare earth elements, which are randomly distributed in the Ln-site. In addition, the relationships between structure and performance are systematically investigated, and the complex chemical bond theory indicates that the Mo–O bond is particularly important for the performances of L5ZMO ceramics. THz-TDS and infrared reflection spectrum analysis together show that ionic polarization is the main polarization contribution in THz/microwave band. Meanwhile, better $Q{\cdot}f$ values can be obtained by optimizing process parameters. Typically, the outstanding dielectric properties with $\varepsilon_r = 10.46$, $Q{\cdot}f = 59{,}713$ GHz, and $\tau_f = -21.94$ ppm/°C are obtained at 750 °C, the temperature stability is optimized effectively compared with the simple $La_2Zr_3(MoO_4)_9$, which indicated that the high-entropy design could improve the temperature stability.

Declaration of competing interest

The authors declare that they have no known competing financial interests or personal relationships that could have appeared to influence the work reported in this paper.

The authors declare the following financial interests/personal relationships which may be considered as potential competing interests.

Acknowledgements

This work was supported by the National Natural Science Foundation of China (No. 51972143). The authors would like to thank the administrators in the infrared beamline workstation of the National Synchrotron Radiation Laboratory for the help in infrared reflection spectrum measurement.

References

[1] Y. Jiang, H. Liu, R. Muhammad, X.J. Luo, K.X. Song, M.M. Mao, S.K. Sun, H. B. Bafrooei, E. Taheri-Nassaj, Y. Iqbal, R. Sun, D.W. Wang, Broadband and high-efficiency of garnet-typed ceramic dielectric resonator antenna for 5G/6G communication application, Ceram. Int. 48 (2022) 26922–26927, https://doi.org/10.1016/j.ceramint.2022.05.396.

[2] Z.F. Liu, Y.Q. Lu, M.S. Ma, Y.R. Zhang, J.J. Feng, Current status and development trend of cold sintering process, J. Inorg. Mater. 38 (2023) 125–136, https://doi.org/10.15541/jim20220338.

[3] C.Q. Zhu, Z.M. Cai, X.H. Cao, Z.X. Fu, L.T. Li, X.H. Wang, High-dielectric-constant nanograin $BaTiO_3$-based ceramics for ultra-thin layer multilayer ceramic capacitors via grain grading engineering, Advanced Powder Materials 1 (2022), 100029, https://doi.org/10.1016/j.apmate.2022.01.002.

[4] W.J. Guo, Z.Y. Ma, Y. Luo, Y.G. Chen, Z.X. Yue, L.T. Li, Structure, defects, and microwave dielectric properties of Al-doped and Al/Nd co-doped $Ba_4Nd_{9.33}Ti_{18}O_{54}$ ceramics, J. Adv. Ceram. 11 (2022) 629–640, https://doi.org/10.1007/s40145-021-0564-0.

[5] X. Huang, H.X. Guo, P.S. Zhu, L. Liu, J. Xiao, D.P. Tang, C. Lin, X. Wu, X.H. Zheng, Microwave dielectric properties of $CaCu_3Ti_4O_{12}$ ceramics: a clue to its intrinsic dielectric response, J. Adv. Dielectr. 13 (2023), 2344001, https://doi.org/10.1142/s2010135x23440010.

[6] H.Y. Yang, L. Chai, G.C. Liang, M.J. Xing, Z.X. Fang, X. Zhang, T.Y. Qin, E.Z. Li, Structure, far-infrared spectroscopy, microwave dielectric properties, and improved low-temperature sintering characteristics of tri-rutile $Mg_{0.5}Ti_{0.5}TaO_4$ ceramics, J. Adv. Ceram. 12 (2023) 296–308, https://doi.org/10.26599/jac.2023.9220683.

[7] G.G. Yao, J.Y. Zhao, Y. Lu, H.K. Liu, C.J. Pei, Q. Ding, M. Chen, Y.M. Zhang, D. Li, F. Wang, Microwave dielectric properties of Li_3TiO_3F oxyfluorides ceramics, Crystals 13 (2023) 897, https://doi.org/10.3390/cryst13060897.

[8] R.U. Khan, I. Khan, B. Ali, R. Muhammad, A. Samad, A. Shah, K.X. Song, D. W. Wang, Structural, dielectric, optical, and electrochemical performance of $Li_4Mo_5O_{17}$ for ULTCC applications, Mater. Res. Bull. 160 (2023), 112142, https://doi.org/10.1016/j.materresbull.2022.112142.

[9] R. Peng, Y.C. Lu, Q. Zhang, Y.M. Lai, G.L. Yu, X.H. Wu, Y.X. Li, H. Su, H.W. Zhang, Amelioration of sintering and multi-frequency dielectric properties of $Mg_3B_2O_6$: a mechanism study of nickel substitution using DFT calculation, J. Adv. Ceram. 10 (2021) 1398–1407, https://doi.org/10.1007/s40145-021-0515-9.

[10] G.Q. He, Y.J. Liu, H.F. Zhou, X.L. Chen, Sintering behavior, phase composition, microstructure, and dielectric characteristics of garnet-type $Ca_3Fe_2Ge_3O_{12}$ microwave ceramics, J. Materiomics (2023), https://doi.org/10.1016/j.jmat.2022.12.005.

[11] C.J. Pei, J.J. Tan, Y. Li, G.G. Yao, Y.M. Jia, Z.Y. Ren, P. Liu, H.W. Zhang, Effect of Sb-site nonstoichiometry on the structure and microwave dielectric properties of $Li_3Mg_2Sb_{1-x}O_6$ ceramics, J. Adv. Ceram. 9 (2020) 588–594, https://doi.org/10.1007/s40145-020-0397-2.

[12] W.J. Luo, S. Yan, J. Zhou, Ceramic-based dielectric metamaterials, Interdiscip. Mater. 1 (2022) 11–27, https://doi.org/10.1002/idm2.12012.

[13] C.Z. Yin, Z.Z. Yu, L.L. Shu, L.J. Liu, Y. Chen, C.C. Li, A low-firing melilite ceramic $Ba_2CuGe_2O_7$ and compositional modulation on microwave dielectric properties through Mg substitution, J. Adv. Ceram. 10 (2020) 108–119, https://doi.org/10.1007/s40145-020-0424-3.

[14] J.Y. Zhang, J. Li, Y.H. Sun, L. Fang, Densification, microwave dielectric properties and rattling effect of $LiYbO_2$ ceramics with low ε_r and anomalous positive τ_f, J. Eur. Ceram. Soc. 42 (2022) 745–7460, https://doi.org/10.1016/j.jeurceramsoc.2022.09.010.

[15] H.C. Yang, S.R. Zhang, H.Y. Yang, Q.Y. Wen, Q. Yang, L. Gui, Q. Zhao, E.Z. Li, The latest process and challenges of microwave dielectric ceramics based on pseudo phase diagrams, J. Adv. Ceram. 10 (2021) 885–932, https://doi.org/10.1007/s40145-021-0528-4.

[16] L.C. Fan, Y.X. Li, J. Li, Q.J. Xiang, X.H. Wang, T.L. Wen, Z.Y. Zhong, Y.L. Liao, High entropy dielectrics, J. Adv. Dielectr. 13 (2023), 2350014, https://doi.org/10.1142/s2010135x23500145.

[17] B.L. Ye, T.Q. Wen, M.C. Nguyen, L.Y. Hao, C.Z. Wang, Y.H. Chu, First-principles study, fabrication and characterization of $(Zr_{0.25}Nb_{0.25}Ti_{0.25}V_{0.25})C$ high-entropy ceramics, Acta Mater. 170 (2019) 15–23, https://doi.org/10.1016/j.actamat.2019.03.021.

[18] W.J. Zhao, F. Yang, Z.L. Liu, H. Chen, Z.H. Shao, X.S. Zhang, K.X. Wang, L.Y. Xue, A novel $(La_{0.2}Sm_{0.2}Eu_{0.2}Gd_{0.2}Tm_{0.2})_2Zr_2O_7$ high-entropy ceramic nanofiber with excellent thermal stability, Ceram. Int. 47 (2021) 29379–29385, https://doi.org/10.1016/j.ceramint.2021.07.105.

[19] D.B. Liu, B.L. Shi, L.Y. Geng, Y.G. Wang, B.S. Xu, Y.F. Chen, High-entropy rare-earth zirconate ceramics with low thermal conductivity for advanced thermal-barrier coatings, J. Adv. Ceram. 11 (2022) 961–973, https://doi.org/10.1007/s40145-022-0589-z.

[20] H.C. Xiang, L. Yao, J.Q. Chen, A.H. Yang, H.T. Yang, L. Fang, Microwave dielectric high-entropy ceramic $Li(Gd_{0.2}Ho_{0.2}Er_{0.2}Yb_{0.2}Lu_{0.2})GeO_4$ with stable temperature coefficient for low-temperature cofired ceramic technologies, J. Mater. Sci. Technol. 93 (2021) 28–32, https://doi.org/10.1016/j.jmst.2021.03.057.

[21] Y.H. Ding, L. Liu, R.Z. Guo, L. Li, X.M. Chen, $Hf_{0.25}Zr_{0.25}Sn_{0.25}Ti_{0.25})O_2$ high-entropy ceramics and their microwave dielectric characteristics, J. Am. Ceram. Soc. 105 (2022) 6710–6717, https://doi.org/10.1111/jace.18641.

[22] K. Liu, H.W. Zhang, C. Liu, J. Li, L. Shi, X.Y. Wang, D.N. Zhang, Crystal structure and microwave dielectric properties of $(Mg_{0.2}Ni_{0.2}Zn_{0.2}Co_{0.2}Mn_{0.2})_2SiO_4$ - a novel high-entropy ceramic, Ceram. Int. 48 (2022) 23307–23313, https://doi.org/10.1016/j.ceramint.2022.04.317.

[23] F.L. Lin, B. Liu, C.C. Hu, K.X. Song, Novel high-entropy microwave dielectric ceramics $Sr(La_{0.2}Nd_{0.2}Sm_{0.2}Eu_{0.2}Gd_{0.2})AlO_4$ with excellent temperature stability and mechanical properties, J. Eur. Ceram. Soc. 43 (2023) 2506–2512, https://doi.org/10.1016/j.jeurceramsoc.2023.01.028.

[24] W.Q. Liu, R.Z. Zuo, A novel low-temperature firable $La_2Zr_3(MoO_4)_9$ microwave dielectric ceramic, J. Eur. Ceram. Soc. 38 (2018) 339–342, https://doi.org/10.1016/j.jeurceramsoc.2017.08.023.

[25] W.Q. Liu, R.Z. Zuo, Low temperature fired $Ln_2Zr_3(MoO_4)_9$ (Ln = Sm, Nd) microwave dielectric ceramics, Ceram. Int. 43 (2017) 17229–17232, https://doi.org/10.1016/j.ceramint.2017.09.083.

[26] Y.H. Zhang, J.J. Sun, N. Dai, Z.C. Wu, H.T. Wu, C.H. Yang, Crystal structure, infrared spectra and microwave dielectric properties of novel extra low-temperature fired $Eu_2Zr_3(MoO_4)_9$ ceramics, J. Eur. Ceram. Soc. 39 (2019) 1127–1131, https://doi.org/10.1016/j.jeurceramsoc.2018.12.042.

[27] H.C. Yang, S.R. Zhang, H.Y. Yang, Y. Yuan, E.Z. Li, $Gd_2Zr_3(MoO_4)_9$ microwave dielectric ceramics with trigonal structure for LTCC application, J. Am. Ceram. Soc. 103 (2019) 1131–1139, https://doi.org/10.1111/jace.16744.

[28] B.J. Tao, C.F. Xing, W.F. Wang, H.T. Wu, Y.Y. Zhou, A novel $Ce_2Zr_3(MoO_4)_9$ microwave dielectric ceramic with ultra-low firing temperature, Ceram. Int. 45 (2019) 24675–24683, https://doi.org/10.1016/j.ceramint.2019.08.206.

[29] H.L. Pan, X. Zhou, H.T. Wu, J.L. Du, Z.B. Feng, M. Wübbenhorst, Composition-structure-property relationships in $CeZr_{1.14}Bi_{0.045}A_{0.045}Mo_{4.5}O_{18}$ (A = Nb, Ta and Sb) microwave dielectric ceramics revealed by Raman, far-infrared and terahertz spectra, J. Mater. Res. Technol. 25 (2023) 369–381, https://doi.org/10.1016/j.jmrt.2023.05.237.

[30] B.W. Hakki, P.D. Coleman, A dielectric resonator method of measuring inductive capacities in the millimeter range, IRE T. Microw. Theory 8 (1960) 402–410, https://doi.org/10.1109/TMTT.1960.1124749.
[31] W.E. Courtney, Analysis and evaluation of a method of measuring the complex permittivity and permeability microwave insulators, IEEE Trans. Microw. Theory 18 (1970) 476–485, https://doi.org/10.1109/TMTT.1970.1127271.
[32] J. Krupka, K. Derzakowski, B. Riddle, J. Baker-Jarvis, A dielectric resonator for measurements of complex permittivity of low loss dielectric materials as a function of temperature, Meas. Sci. Technol. 9 (1998) 1751–1756, https://doi.org/10.1088/0957-0233/9/10/015.
[33] M.T. Sebastian, Dielectric Materials for Wireless Communication, Elsevier, Oxford, 2008.
[34] R.D. Shannon, Revised effective ionic radii and systematic studies of interatomic distances in halides and chalcogenides, Acta Crystallogr. A 32 (1976) 751–767, https://doi.org/10.1107/S0567739476001551.
[35] A.J. Bosman, E.E. Havinga, Temperature dependence of dielectric constants of cubic ionic compounds, Phys. Rev. 129 (1963) 1593–1600, https://doi.org/10.1103/PhysRev.129.1593.
[36] R.D. Shannon, G.R. Rossman, Dielectric constants of silicate garnets and the oxide additivity rule, Am. Mineral. 77 (1992) 94–100, https://doi.org/10.1007/BF00306555.
[37] R.D. Shannon, Dielectric polarizabilities of ions in oxides and fluorides, J. Appl. Phys. 73 (1993) 348–366, https://doi.org/10.1063/1.353856.
[38] G.K. Choi, J.R. Kim, S.H. Yoon, K.S. Hong, Microwave dielectric properties of scheelite (A = Ca, Sr, Ba) and wolframite (A = Mg, Zn, Mn) $AMoO_4$ compounds, J. Eur. Ceram. Soc. 27 (2007) 3063–3067, https://doi.org/10.1016/j.jeurceramsoc.2006.11.037.
[39] Z.J. Wu, Q.B. Meng, S.Y. Zhang, Semiempirical study on the valences of Cu and bond covalency in $Y_{1-x}Ca_xBa_2Cu_3O_{6+y}$, Phys. Rev. B 58 (1998) 958–962, https://doi.org/10.1103/PhysRevB.58.958.
[40] G.G. Yao, J.X. Yan, J.J. Tan, C.J. Pei, P. Liu, H.W. Zhang, D.W. Wang, Structure, chemical bond and microwave dielectric characteristics of novel $Li_3Mg_4NbO_8$ ceramics, J. Eur. Ceram. Soc. 41 (2021) 6490–6494, https://doi.org/10.1016/j.jeurceramsoc.2021.06.029.
[41] D.F. Xue, S.Y. Zhang, Calculation of the nonlinear optical coefficient of the $NdAl_3(BO_3)_4$ crystal, J. Phys. Condens. Matter 8 (1996) 1949–1956, https://doi.org/10.1088/0953-8984/8/12/009.
[42] H.Y. Yang, S.R. Zhang, H.C. Yang, E.Z. Li, Usage of P-V-L bond theory in studying the structural/property regulation of microwave dielectric ceramics: a review, Inorg. Chem. Front. 7 (2020) 4711–4753, https://doi.org/10.1039/D0QI00907E.
[43] X. Zhou, L.T. Liu, J.J. Sun, N.K. Zhang, H.Z. Sun, H.T. Wu, W.H. Tao, Effects of $(Mg_{1/3}Sb_{2/3})^{4+}$ substitution on the structure and microwave dielectric properties of $Ce_2Zr_3(MoO_4)_9$ ceramics, J. Adv. Ceram. 10 (2021) 778–789, https://doi.org/10.1007/s40145-021-0472-3.
[44] J. Bao, Y.P. Zhang, H. Kimura, H.T. Wu, Z.X. Yue, Crystal structure, chemical bond characteristics, infrared reflection spectrum, and microwave dielectric properties of $Nd_2(Zr_{1-x}Ti_x)_3(MoO_4)_9$ ceramics, J. Adv. Ceram. 12 (2023) 82–92, https://doi.org/10.26599/jac.2023.9220668.
[45] C. Feng, X. Zhou, B.J. Tao, H.T. Wu, S.F. Huang, Crystal structure and enhanced microwave dielectric properties of the $Ce_2[Zr_{1-x}(Al_{1/2}Ta_{1/2})_x]_3(MoO_4)_9$ ceramics at microwave frequency, J. Adv. Ceram. 11 (2022) 392–402, https://doi.org/10.1007/s40145-021-0541-7.
[46] S.S. Batsanov, Dielectric methods of studying the chemical bond and the concept of electronegativity, Russ. Chem. Rev. 51 (1982) 684–697, https://doi.org/10.1070/RC1982v051n07ABEH002900.
[47] W.J. Guo, Z.Y. Ma, Y.G. Chen, Y.T. Lu, Z.X. Yue, Lattice dynamics and terahertz response of microwave dielectrics: a case study of Al-doped $Ca_{0.6}Sm_{0.27}TiO_3$ ceramics, J. Eur. Ceram. Soc. 42 (2022) 4953–4961, https://doi.org/10.1016/j.jeurceramsoc.2022.05.045.
[48] Y. Luo, W.J. Guo, Y.G. Chen, J. Zhang, Z.X. Yue, Thermally-stimulated defect relaxations and microwave/terahertz dielectric response of La,Al co-doped (Ba,Sr) $La_4Ti_4O_{15}$ ceramics, J. Eur. Ceram. Soc. 41 (2021) 158–164, https://doi.org/10.1016/j.jeurceramsoc.2021.09.016.
[49] L.T. Liu, W.J. Guo, S.J. Yan, P. Liu, J.L. Du, Y.P. Zhang, H.T. Wu, Y.G. Chen, Z. X. Yue, Microstructure, Raman spectroscopy, THz time domain spectrum and microwave dielectric properties of $Li_2Ti_{1-x}(Zn_{1/3}Ta_{2/3})_xO_3$ ceramics, Ceram. Int. 49 (2023) 6864–6872, https://doi.org/10.1016/j.ceramint.2022.10.169.
[50] R.G. Shi, S.K. Zhu, R. Muhammad, T. Zhou, B. Liu, M.M. Mao, D.W. Wang, K. X. Song, Degree of inversion of A/B lattice sites and microwave/millimeter wave/terahertz dielectric properties of $MgAl_{2-x}(Zn_{0.5}Mn_{0.5})_xO_4$ ceramics, J. Eur. Ceram. Soc. 43 (2023) 3324–3330, https://doi.org/10.1016/j.jeurceramsoc.2023.01.020.
[51] Y. Jiang, G.F. Wu, M.M. Mao, R. Muhammad, W.Q. Sheng, B. Liu, H.B. Bafrooei, E. Taheri-Nassaj, K.X. Song, Deeper insights into dodecahedron distortion and microwave dielectric properties of $Y_{3-x}R_xAl_{(Oct)2}Al_{(Tet)3-x}Si_xO_{12}$ (x = 0.1–0.5; R = Mg, Ca) garnet-type ceramics, Ceram. Int. 49 (2023) 23334–23339, https://doi.org/10.1016/j.ceramint.2023.04.165.
[52] K. Wakino, M. Murata, H. Tamura, Far infrared reflection spectra of Ba(Zn, Ta)O_3-$BaZrO_3$ dielectric resonator material, J. Am. Ceram. Soc. 69 (1986) 34–37, https://doi.org/10.7567/JJAPS.24S2.1042.
[53] J. Bao, Y.P. Zhang, H.T. Wu, Y.Y. Zhou, Z.X. Yue, Sintering characteristics, crystal structure and dielectric properties of cobalt-tungsten doped molybdate-based ceramics at microwave frequency, J. Materiomics 8 (2022) 949–957, https://doi.org/10.1016/j.jmat.2022.04.004.
[54] C.F. Xing, Y.H. Zhang, B.J. Tao, H.T. Wu, Y.Y. Zhou, Crystal structure, infrared spectra and microwave dielectric properties of low-firing $La_2Zr_3(MoO_4)_9$ ceramics prepared by reaction-sintering process, Ceram. Int. 45 (2019) 22376–22382, https://doi.org/10.1016/j.ceramint.2019.07.142.
[55] Y. Tang, M.Y. Xu, L. Duan, J.Q. Chen, C.C. Li, H.C. Xiang, L. Fang, Structure, microwave dielectric properties, and infrared reflectivity spectrum of olivine type Ca_2GeO_4 ceramic, J. Eur. Ceram. Soc. 39 (2019) 2354–2359, https://doi.org/10.1016/j.jeurceramsoc.2019.02.039.
[56] H.R. Tian, J.J. Zheng, L.T. Liu, H.T. Wu, H. Kimura, Y.Z. Lu, Z.X. Yue, Structure characteristics and microwave dielectric properties of $Pr_2(Zr_{1-x}Ti_x)_3(MoO_4)_9$ solid solution ceramic with a stable temperature coefficient, J. Mater. Sci. Technol. 116 (2022) 121–129, https://doi.org/10.1016/j.jmst.2021.10.051.
[57] B. Liu, Y.H. Huang, H.B. Bafrooei, K.X. Song, L. Li, X.M. Chen, Effects of structural transition on microwave dielectric properties of $Sr_3(Ti_{1-x}Sn_x)_2O_7$ ceramics, J. Eur. Ceram. Soc. 39 (2019) 4794–4799, https://doi.org/10.1016/j.jeurceramsoc.2019.07.046.
[58] M.M. Mao, X.Q. Liu, X.M. Chen, Structural evolution and its effects on dielectric loss in $Sr_{1+x}Sm_{1-x}Al_{1-x}Ti_xO_4$ microwave dielectric ceramics, J. Am. Ceram. Soc. 94 (2011) 2506–2511, https://doi.org/10.1111/j.1551-2916.2011.04408.x.